Ki-Ju Kang
Seon-Ho Choi
Department of Mechanical Engineering,
Chonnam National University,
Kwangju 500-757, Republic of Korea

Tae-Sung Bae
Department of Dental Materials and Institute of Oral Bioscience,
Chonbuk National University,
Chonju 561-756, Republic of Korea

Near-Threshold Fatigue Crack Growth at 63Sn37Pb Solder Joints

Fatigue tests were performed using single lap-joint specimens to obtain near-threshold fatigue crack growth data of solder joint under mode-II load. Attention was focused on the effect of high temperature aging and microstructures separately from the intermetallics. As a result, it was shown that the long cast time yielded the intermetallics and microstructures of the solder invariable regardless of aging condition. The granular microstructure of the air-cooled specimens was shown to be inferior to the laminated microstructure of the furnace-cooled specimens. Also, transition of fatigue crack behavior with ΔJ and the procedure of fatigue crack propagation from the pre-crack tip were discussed.
[DOI: 10.1115/1.1510863]

1 Introduction

As solder joints with smaller and smaller feature size are being incorporated in the electronics packages, the long-term reliability of solder joints becomes a hot issue. A key factor of the solder joint failure is the difference of thermal expansion between the individual components, which induces thermal low cycle fatigue. Most research on reliability of solder joints has been focused on the low cycle fatigue. Those were well reviewed by Lau [1] and Frear et al. [2]. Electronic packages, however often experience mechanical load such as shocks and vibrations as well. Particularly for automotive, military and avionics applications, the fatigue resistance against vibration loads is very important. A few works have been performed on it (McKeown [3]; Sidharth and Baker [4]).

McKeown [3] has estimated fatigue life of solder joints with leadless and leaded chip carriers under vibration. He used a traditional S-N curve, which had been empirically obtained using the actual components mounted on a PWB. Sidharth and Baker [4] have performed sophisticated FEA (finite element analysis) to calculate the stresses of corner leads of peripheral leaded components under vibration bending moment, which in turn was used to estimate the fatigue life through the S-N curve. However, the approaches using S-N curves have drawbacks as follows; First, the S-N curve does not count the size effect. Time taken for a fatigue crack to propagate till the final fracture, which is a major portion of the total fatigue life, obviously depends on the size. Especially for the solder joints whose dimensions are being shrunk, a S-N curve obtained according to the previous standard likely gives over-estimation of the fatigue life. Second, the S-N curve does not count existence of a crack. No joint can be guaranteed to be perfectly free of defects. Cold soldering, poor surface preparation or inhomogeneous heating in surface mounting process can lead to imperfect bonding and an interface crack is created. The failure of a single solder joint could render an entire electronic assembly inoperable. Therefore, it is reasonable to assume existence of a crack undetectable, and to consider propagation of the crack in order to assess the integrity of the circuitry.

Logsdon et al. [5] and Cutiongco et al. [6] have done the experiments of fatigue crack propagation and low cycle fatigue of a bulk solder, respectively. However, near the interface with copper leads or patterns on PWB, intermetallics such as Cu_3Sn or Cu_6Sn_5 form, which could affect the fatigue behavior. Fatigue crack growth rate in solder joints has been measured by Guo and Conrad [7]. They found that, under shear loading, the fatigue crack initiated at the centrally located notches soon wandered forward the solder/Cu interface and then propagated in the solder adjacent to the intermetallics compound. Other research on the fatigue crack growth near the solder interface is rare, especially for the threshold region of the growth rates, which would be a major interest for fatigue design against vibration loads. This work was carried out to explore the fatigue crack behavior adjacent the interface of solder joints in the threshold region under mode-II loading.

2 Experiments and Numerical Analysis

2.1 Specimen Preparation. The solder alloy employed was commercial 63Sn37Pb. The substrates were made of oxygen-free brass. The mechanical properties used for finite element analysis, which will be mentioned below, are listed in Table 1. A pre-crack along the interface was produced by vapor-depositing a 0.2 μm layer of aluminum onto one third of the bonding surface of one of the substrate prior to soldering. After vapor deposition poor adhesion between this aluminum layer and the solder was assured by oxidizing the aluminum at 400°C for 1 h in an electric furnace. In order to let thick intermetallics develop along the interfaces, the substrates and solder assembly was cast at 220°C for 4 h in a vacuum furnace. Voids within the solder were extracted by repeated vacuum-degassing. Detailed description of the specimen preparation is given in Choi et al., [8]. Three series of specimens were prepared to investigate the effects of the cooling rate after soldering and long time exposure to high temperature (150°C/200 h). Specimens of series A were air-cooled in room temperature, then exposed to the high temperature in an elective oven. Specimens of series B were slow-cooled (−1°C/mm) in a furnace. Specimens of series C were slow-cooled, then exposed to the high temperature. All the conditions of the cooling and aging are listed in Table 2. Finally, the cast brass/solder combination was machined to the single-lap-joint geometry as shown in Fig. 1. The solder layer thickness was 0.3 mm and the pre-crack length was 1 mm.

2.2 Experimental Procedures. A schematic diagram of the fatigue test system is shown in Fig. 2. Pure shear loading was applied to the specimens by an electro-magnetic actuator, which came from a loudspeaker. The detailed description of the system is given in the reference (Song et al. [9]). In order to avoid heating up during sinusoidal loading with nonzero mean, ferro-fluid (trade mark Ferrofluidics Co., Nashua, NH) was injected into the gap between bobbin coil and magnet pole, and the actuator was air cooled by an electric fan. The maximum loads were 65 and 85 N. The load ratio was $R=0$, and the frequency was 20 Hz. In order to minimize bending moment applied, the specimens were loaded via a pair of universal joints. Crack length was measured by an

Contributed by the Electronic and Photonic Packaging Division for publication in the JOURNAL OF ELECTRONIC PACKAGING. Manuscript received by the EPPD Division October 12, 2001. Associate Editor: Y.-H. Pao.

 Copyright © 2002 by ASME

Downloaded From: https://electronicpackaging.asmedigitalcollection.asme.org on 06/28/2019 Terms of Use: http://www.asme.org/about-asme/terms-of-use

Table 1 Material properties of brass and solder

Materials / Properties	Brass	Solder
Composition	Oxygen free Brass	63Sn37Pb
Tensile strength (Mpa)	305	35
Young's modulus (Gpa)	90	15
Poisson's ratio	0.35	0.397

optical microscope (×1000, Zeiss Axiotech 100HD). The data of crack length versus number of cycles were reduced by the 7-point incremental polynomial technique to give the crack propagation rates. All tests were performed in ambient air (22°C, 55%RH).

2.3 Numerical Analyses. Finite element analyses (FEA) were performed to calculate the fracture parameters mode mix and J-integral. The mode mix ψ was defined as ratio of shear stress σ_{12} to normal stress σ_{22} at a distance ℓ_1 along the cracked plane ahead of the crack tip (Hutchinson and Suo [10]). That is

$$\psi = \tan^{-1}\left(\frac{\sigma_{12}}{\sigma_{22}}\right)\Bigg|_{r=\ell_1, \theta=0°}$$

where r is the distance from the crack tip and θ is the angle from the cracked plane. Figure 3 shows a model for FEA. The total numbers of elements were 1538 to 1624. The element type was 8-node biquadratic, reduced integration plane strain element (CPE8R). The plastic deformation of the solder was described by J_2-deformation theory of plasticity. Finite element calculations for stress-strain and J-integral were performed using the commercial software ABAQUS [11].

Figure 4 shows variation of the mode mix ψ with the crack length. In the entire range of crack length, i.e., $a/w = 0.36$a/w=0.36∼0.66. The mode mix varies from −45° to −38° in spite of pure mode-II loading applied. Variation of J-integral is shown in Fig. 5. As the crack length increases, J-integral increases exponentially under a constant load.

Table 2 Cooling and aging conditions for the specimens of series A to C

Series	Air-cooled	Furnace-cooled	High temperature aging (150 °C/200hrs)
A	∨		∨
B		∨	
C		∨	∨

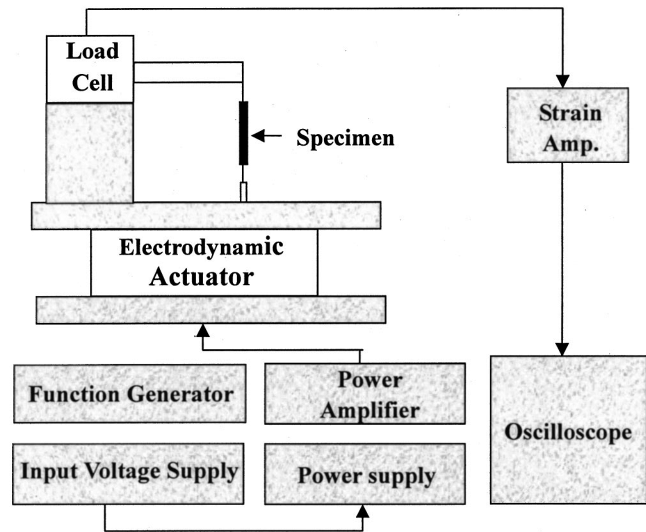

Fig. 2 Schematic diagram of the fatigue test system

3 Results and Discussion

3.1 Microstructures. The microstructures of the solder in the specimens of series A to C are shown in Fig. 6. Granular microstructures form in the air cooled specimens (Fig. 6(*a*)). In contrast, in the slow cooled specimens, the laminated microstructures form (Fig. 6(*b*)). The cast time during specimen preparation was so long that the intermetallics Cu_3Sn as well as Cu_6Sn_5 had developed fully (thickness≈10 μm), as shown in Fig. 7. Therefore, the intermetallics remained unchanged in the thickness and the composition regardless of cooling rate or even aging condition. The microstructures of the solder also were quite stable. Even the high temperature aging (150°C/200 h) did not make any significant change as shown in Fig. 6(*c*). This is quite striking. Previous research, for example, Lampe [12], has shown that aging let a bulk solder be recrystallized into an equiaxed structure and coarsened, and intermetallics grew in thickness and the Pb-rich

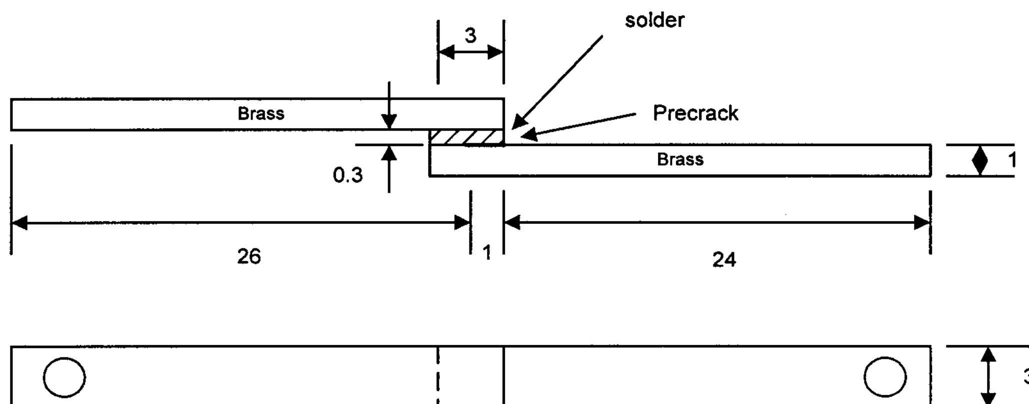

Fig. 1 Configurations of single-lap-joint specimen

Downloaded From: https://electronicpackaging.asmedigitalcollection.asme.org on 06/28/2019 Terms of Use: http://www.asme.org/about-asme/terms-of-use

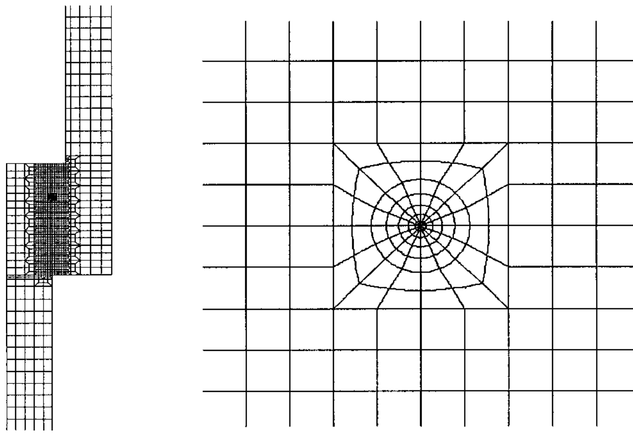

Fig. 3 Finite element model of the single-lap-joint specimen

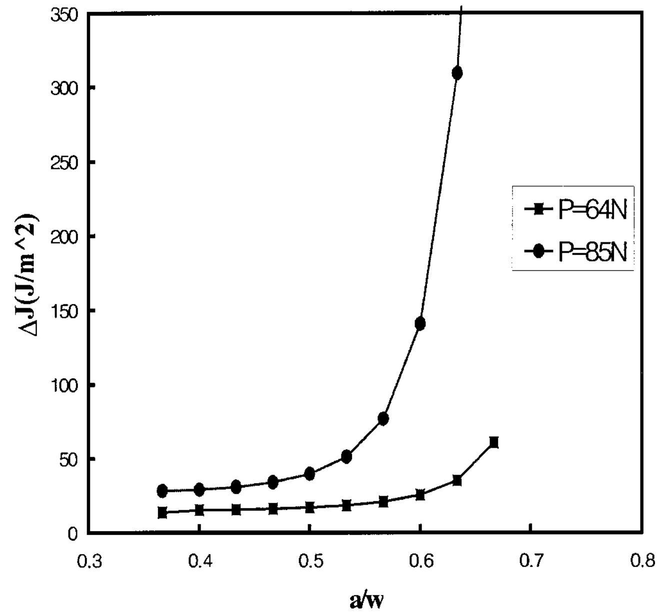

Fig. 5 Variation of *J*-integral with the crack length under constant load control

phase developed even in room temperature. The stableness of the microstructure under long time exposure to high temperature may be a great merit in electronics packages applications. Some more research is needed to explore the mechanism.

3.2 Fatigue Crack Propagation. A typical example of the fatigue crack behavior is shown in Fig. 8. First, the crack grew rapidly from the pre-cracked tip along a path between the Cu_3Sn layer and the solder. Stress concentrated at the sharp crack tip easily broke the brittle Cu_6Sn_5 grains protruding into the solder, which is believed to result in the fast propagation. The strange rough surface whose magnified views are given in Figs. 8(*b*) and (*c*) is regarded as a consequence of severe plastic deformation due to the stress concentration. In fact the width of the rough surface is comparable to the plastic zone size estimated by the finite element analysis for the sharp-cracked specimen.

After some advance the fatigue crack took a new path into the Pb-rich phase just above the Cu_6Sn_5 grains, as shown in Fig. 8; stable crack propagation at the slower rate followed. Simultaneously, a few micro-cracks were created along the interfaces between the Pb-rich phase grains and the Sn-rich phase grains in the solder adjacent to the main crack. Figure 9 shows an example of the stable crack growth.

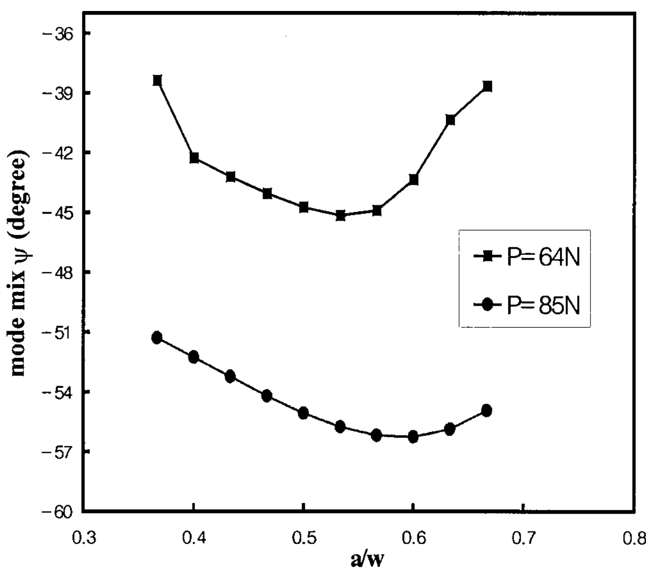

Fig. 4 Variation of mode mix with the crack length under constant load control

As the crack tip encountered a solder colony in which the Sn-rich phases grains and Pb-rich phases grains were parallel arranged in a direction perpendicular to the main crack path, the crack propagation was significantly retarded and several micro-cracks were created and grew independently of the main crack. Then some of them propagated along the colony boundaries, as shown in Fig. 10, and the main crack was virtually stopped. In some specimens another crack was initiated from the nonpre-cracked opposite corner of the specimen and grew. The fatigue crack behavior schematically illustrated in Fig. 11. That is, the fatigue crack propagation is classified into the three stages as follows; Stage 1, fast crack growth from the pre-crack tip along the path between Cu_3Sn layer and the solder. Stage 2, the stable crack growth along the Pb-rich phase just above the Cu_6Sn_5 grains. Stage 3, main crack retardation with colony boundary cracking.

The experimental results of the fatigue crack growth rate versus ΔJ are summarized in Fig. 12. For the purpose of comparison, the results by Logsdon et al. [5] for a bulk solder under mode-I loading and the results by Guo and Conrad [7] for a solder joint under mode-II loading are plotted together. Remember that all the specimens of series A to C have the same intermetallics in the thickness and the composition. Virtually no difference in the fatigue propagation behavior is found between the series B and C, that is, the high temperature aging did not have any significant effects. However, the cooling rate after casting gave substantial effect. That is, the granular micro-structure of the air cooled specimens of series A is inferior to the laminated micro-structure of the furnace cooled specimens of series B or C. The reason can be explained by the mechanism of crack retardation mentioned earlier.

Morris et al. [13] have shown that the Pb-rich phase adjacent to the intermetallics is the main path for a fatigue crack to go through under mode-II loading and that the micro-structure of the solder has minor effect on the fatigue crack propagation rate. In this work only structural sensitivity was explored separately using the specimens with the constant intermetallics. Yao and Shang [14] have performed fatigue tests for solder/copper interfaces in flexural peel mode. The mode mix at a distance of $\ell_1 = 0.03$ mm was about 40°, which is almost the same as the one in this work.

Downloaded From: https://electronicpackaging.asmedigitalcollection.asme.org on 06/28/2019 Terms of Use: http://www.asme.org/about-asme/terms-of-use

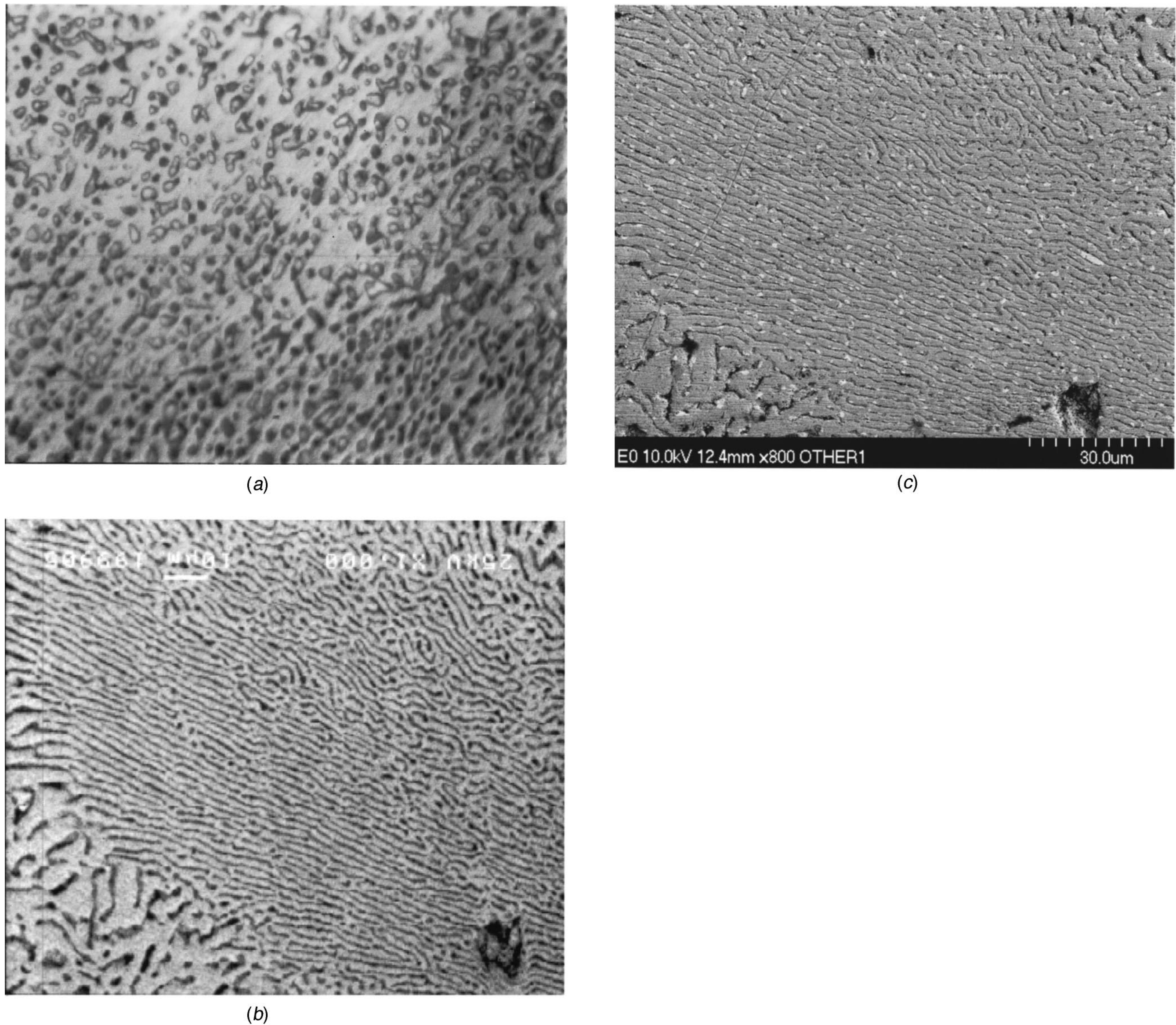

Fig. 6 Microstructures of the solder in the specimens of (*a*) series A: air cooled and aged at 150°C/200 h, (*b*) series B: furnace cooled and aged at room temperature; and (*c*) series C: furnace cooled and aged at 150°C/200 h

In threshold region of fatigue growth, their results of the specimens aged at high temperature (170°C/7 days) are quite similar to the ones of the series B or C shown in Fig. 12. However, in regions of $da/dN \geqslant 10^{-6}$ mm/cycle, their results deviate from the ones in this work, that is, the fatigue crack growth rate kept increasing with ΔJ. The grain coarsening due to the high temperature aging, which did not happen in this work as shown in Fig. 6, is believed to make the discrepancy.

We believe that the fatigue crack growth mechanism is completely changed near $\Delta J \approx 1000$ J/m^2. Thereafter the fatigue crack mode gets transgranular with no clear micro-structural preference, as shown by Guo and Conrad [7]. In the range of $100 < \Delta J < 1000$ J/m^2, as mentioned above, the fatigue crack was retarded by energy dissipation due to the minor cracks along weak interfaces between Pb-rich phase grains and Sn-rich phase grains, which can be regarded as the barrier defined by Miller [15] against transition to the transgranular crack growth.

The most striking thing in Fig. 12 is that the fatigue crack growth rate of a bulk solder under mode-I loading [5] in the threshold region is very similar to the ones of the solder/brass interface under mode-II loading. The reason is left to be solved.

4 Conclusions

The near-threshold fatigue crack behavior along the interface of solder joints has been explored using single-lap-joint specimens under mode-II loading. Attention was focused on the effect of only micro-structures separately from the intermetallics. As a result, the following conclusions have been obtained:

1. Long cast time yields the intermetallics invariable in the thickness and the composition regardless of cooling rate or even aging condition. The micro-structures of the solder also are quite stable even under the high temperature aging (150°C/200 h).
2. The fatigue crack propagation is classified into the three stages as follows; Stage 1, fast crack growth from the pre-crack tip along the path between Cu_3Sn layer and the solder.

Downloaded From: https://electronicpackaging.asmedigitalcollection.asme.org on 06/28/2019 Terms of Use: http://www.asme.org/about-asme/terms-of-use

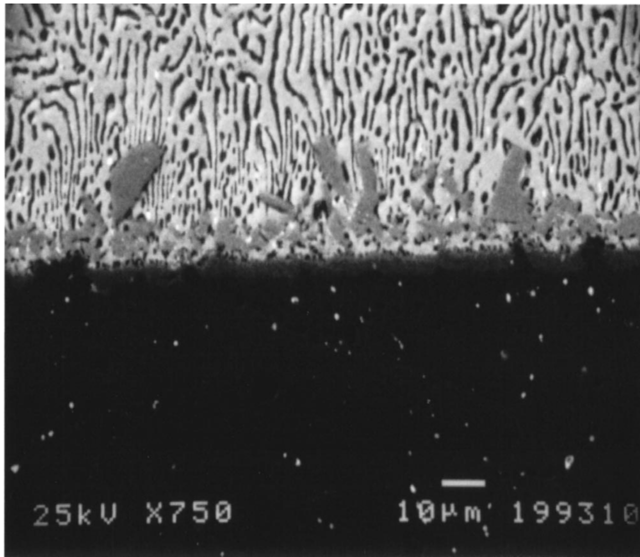

Fig. 7 Scanning electron micrographs of microstructure near the interface

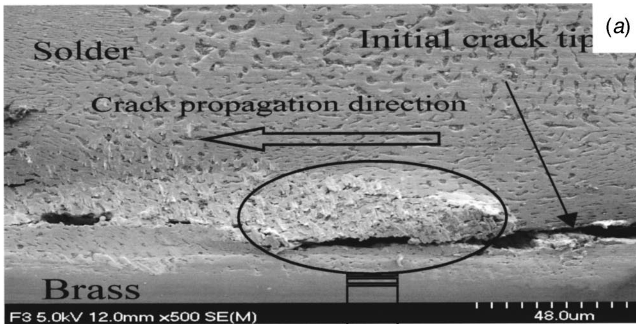

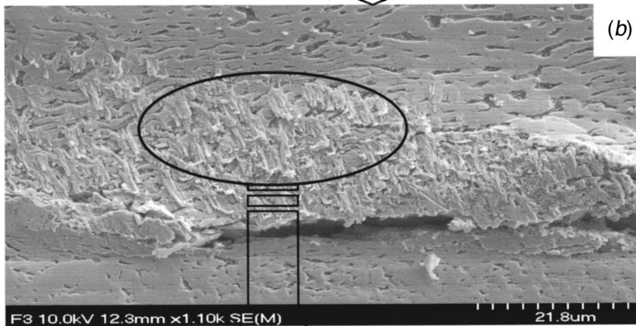

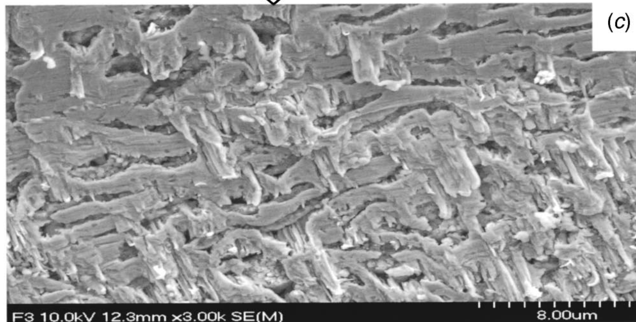

Fig. 8 Scanning electron micrographs of fatigue crack growth from the pre-crack tip—(*a*) a general view; (*b*) and (*c*) magnified views of the strange rough surface developed on the lateral surface at the initial stage of crack growth

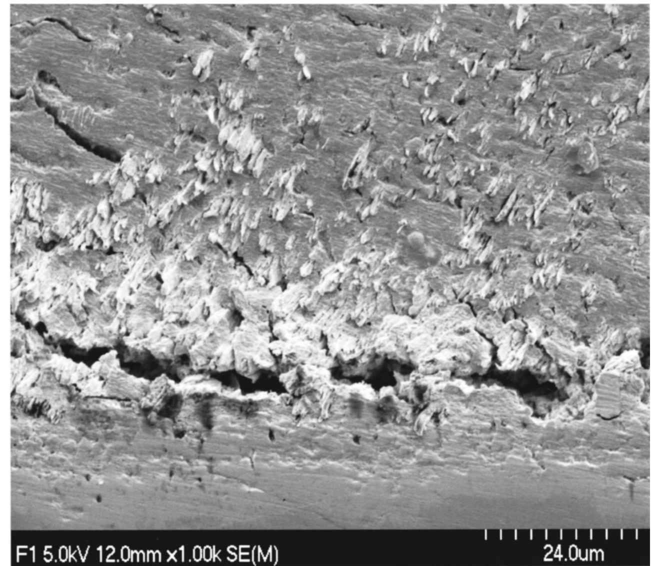

Fig. 9 The main crack path and some micro-cracks developed nearby

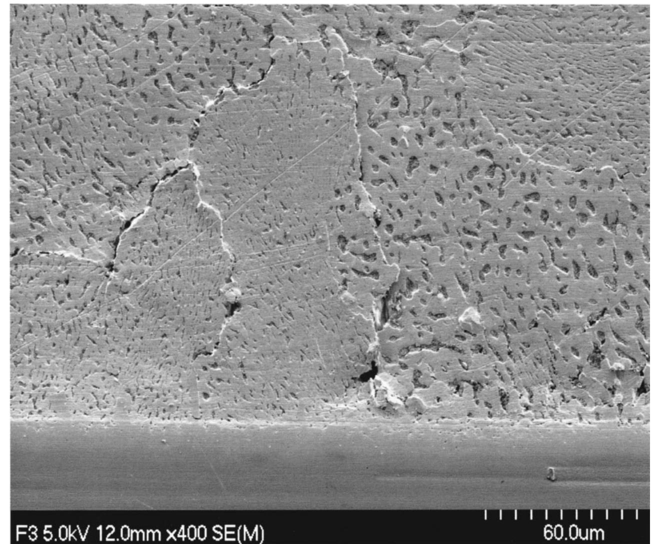

Fig. 10 Cracks propagated along the colony boundaries

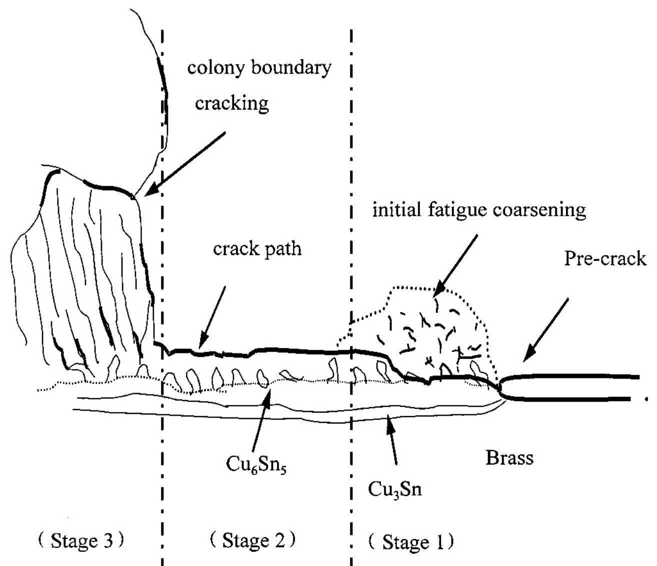

Fig. 11 A schematic diagram of the three stages of crack propagation near the interface of solder joints

Downloaded From: https://electronicpackaging.asmedigitalcollection.asme.org on 06/28/2019 Terms of Use: http://www.asme.org/about-asme/terms-of-use

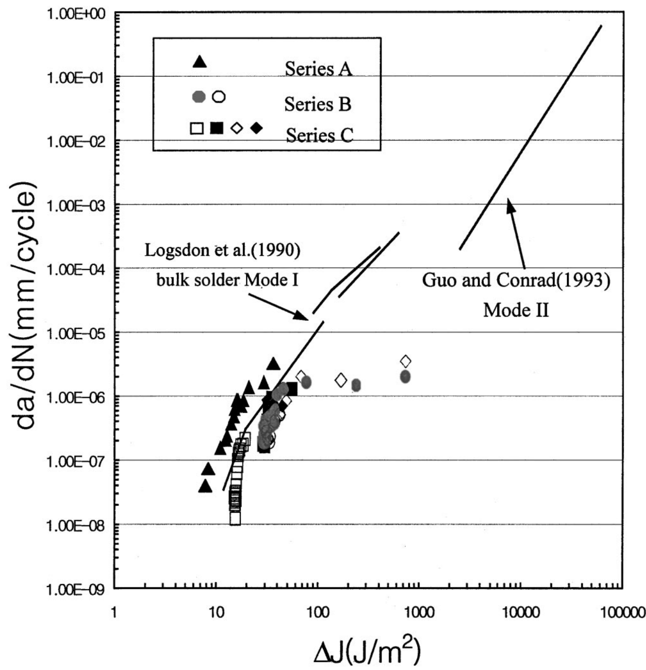

Fig. 12 Experimental results of the fatigue crack growth rate versus ΔJ

Stage 2, the stable crack growth along the Pb-rich phase just above the Cu_6Sn_5 grains. Stage 3, main crack retardation with colony boundary cracking.

3. The fatigue crack growth mechanism is completely changed near $\Delta J \approx 1000\ J/m^2$. Thereafter the fatigue crack mode gets transgranular with no clear micro-structural preference.
4. The cooling rate after casting has substantial effect on fatigue crack behavior. The granular micro-structure of the air cooled specimens is inferior to the laminated micro-structure of the furnace cooled specimens.

Acknowledgment

This research was supported by Chonnam National University Foundation through a grant of sabbatical year research. The authors are grateful to Mr. Sang-Chai Lim for plotting the figures and typing.

References

[1] Lau, J. H., 1991, *Solder Joint Reliability*, Van Nostrand Reinhold, New York, NY.
[2] Frear, D. R., Burchett, S. N., and Morgan, H. S., 1994, *The Mechanics of Solder Alloy Interconnects*, Van Nostrand Reinhold, New York, NY.
[3] McKeown, S. A., 1993, "Solder Life Prediction of Leadless and Leaded Surface Mount Components Under Thermal Cycling and Vibration," *Adv. Electronic Packaging*, EEP-Vol. 4-2, pp. 987–994.
[4] Sidharth, and Baker, D. B., 1996, "Vibration Induced Fatigue Life Estimation of Corner Leads of Peripheral Leaded Components," ASME J. Electron. Packag., **118**, pp. 244–249.
[5] Logsdon, W. A., Liaw, P. K., and Burke, M. A., 1990, "Fracture Behavior of 63Sn-37Pb Solder," Eng. Fract. Mech., **36**, pp. 183–218.
[6] Cutiongco, E. C., Vaynman, S., Fine, M. E., and Jeannotte, D. A., 1990, "Isothermal Fatigue of 63Sn-37Pb Solder," ASME J. Electron. Packag., **112**, pp. 110–114.
[7] Guo, Z., and Conrad, H., 1993, "Fatigue Crack Growth Rate in 63Sn37Pb Solder Joints," ASME J. Electron. Packag., **115**, pp. 159–164.
[8] Choi, S. H., Song, B. G., Kang, K. J., and Fleck, N. A., 2001, "Fracture of a Ductile Layer Constrained by Stiff Substrates," Fatigue Fract. Eng. Mater. Struct., **23**, pp. 1–13.
[9] Song, J. H., Shin, Y. S., and Im, Y. S., 1989, "Construction of Small Sized, Electro-Dynamic Type Bending Fatigue Testing Machine," in Korean KSME Trans. A, **13(1)**, pp. 199–203.
[10] Hutchinson, J. W., and Suo, Z., 1991, "Mixed Mode Cracking in Layered Materials," Adv. Appl. Mech., **28**, pp. 1–21.
[11] ABAQUS, 1996, *User's Manual*, Version 5.6, HKS Inc.
[12] Lampe, B. T., 1976, "Room Temperature Aging Properties of Some Solder Alloys," Welding Research Supplement, p. 330-s–340-s.
[13] Morris, J. W., Jr., Goldstein, J. L. F., and Mei, Z., 1994, "Microstructual Influences on the mechanical properties of solder," *The Mechanics of Solder Alloy Interconnects*, eds., D. R. Frear, S. N. Burchett, and H. S. Morgan, Van Nostrand Reinhold, pp. 7–41.
[14] Yao, D., and Shang, J. K., 1995, "Effect of Aging on Fatigue Crack Growth at Sn-Pb/Cu Interfaces," Metall. Mater. Trans. A, **26A**, pp. 2677–2685.
[15] Miller, K. J., 1991, "Metal Fatigue—Past, Current and Future," I Mech E Conf. Publ., **205**, pp. 1–14.

Downloaded From: https://electronicpackaging.asmedigitalcollection.asme.org on 06/28/2019 Terms of Use: http://www.asme.org/about-asme/terms-of-use